Comparison between 1D and 2D numerical models of a multi-tubular packed-bed reactor for methanol steam reforming

Zhu, Jimin; Cui, Xiaoti; Simon Araya, Samuel

Published in:
International Journal of Hydrogen Energy

DOI (link to publication from Publisher):
10.1016/j.ijhydene.2022.05.109

Publication date:
2022

Document Version
Publisher's PDF, also known as Version of record

Available online at www.sciencedirect.com

ScienceDirect

journal homepage: www.elsevier.com/locate/he

Comparison between 1D and 2D numerical models of a multi-tubular packed-bed reactor for methanol steam reforming

Jimin Zhu[*], *Xiaoti Cui*, *Samuel Simon Araya*

AAU Energy, Aalborg University, Pontoppidanstræde 111, 9220, Aalborg, Denmark

HIGHLIGHTS

- Development of a 2D model for the MSR in a multi-tubular packed-bed reactor.
- Comparison of simulation results between 1D and 2D reactor models.
- Prediction of the temperature distribution inside a reactor tube.
- Studying the effects of geometry and operating conditions on reformer performance.
- Optimization of operating conditions for integration with a 5 kW HT-PEMFC stack.

GRAPHICAL ABSTRACT

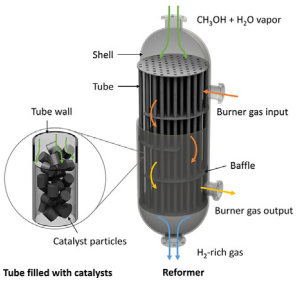

ARTICLE INFO

Article history:
Received 31 January 2022
Received in revised form
22 April 2022
Accepted 12 May 2022
Available online xxx

Keywords:
Methanol steam reforming
Hydrogen production
Packed-bed reactor
Thermal behaviour
Reactor modelling

ABSTRACT

The hydrogen-rich gas produced in-situ by methanol steam reforming (MSR) reactions significantly affects the performance and endurance of the high-temperature polymer electrolyte membrane (HT-PEM) fuel cell stack. A numerical study of MSR reactions over a commercial $CuO/ZnO/Al_2O_3$ catalyst coupling with the heat and mass transfer phenomena in a co-current packed-bed reactor is conducted. The simulation results of a 1D and a 2D pseudo-homogeneous reactor model are compared, which indicates the importance of radial gradients in the catalyst bed. The effects of geometry and operating parameters on the steady-state performance of the reactor are investigated. The simulation results show that the increases in the inlet temperature of burner gas and the tube diameter significantly increase the non-uniformity of radial temperature distributions in reformer tubes. Hot spots are formed near the tube wall in the entrance region. The hot-spot temperature in the catalyst bed rises with the increase in the inlet temperature of burner gas. Moreover, the difference in simulation results between the 1D and 2D models is shown to be primarily influenced by the tube diameter. With a methanol conversion approaching 100% or a relatively small tube diameter, the simplified 1D model can be used instead of the 2D model to estimate the reactor performance.

* *Corresponding author.*
E-mail address: jzu@energy.aau.dk (J. Zhu).

https://doi.org/10.1016/j.ijhydene.2022.05.109

Introduction

Hydrogen is a clean and renewable energy source that plays an essential role in hydrogen-based energy systems, especially in polymer electrolyte membrane (PEM) fuel cell systems. As we know, the PEM fuel cell is a compact electrochemical device that converts the chemical energy in hydrogen and oxygen to electrical energy with high energy efficiency and zero-pollutant emission. According to their ranges of operating temperature, PEM fuel cells can be classified into two categories. The low-temperature polymer electrolyte membrane (LT-PEM) fuel cell generally operates at a temperature below 373 K. This low operating temperature makes a rapid start-up possible but also leads to a high requirement for hydrogen purity. The high-temperature polymer electrolyte membrane (HT-PEM) fuel cell operates at 393 – 473 K. By operating at a higher temperature, the HT-PEM fuel cell gets an improved tolerance towards carbon monoxide (CO) up to 3– 5% vol [1], making it suitable to be integrated with an in-situ hydrogen production system without purification.

Methanol stands out among various hydrogen carriers because it is in liquid form under standard conditions and has a high hydrogen to carbon ratio (4 : 1). The high energy density and stability of methanol at ambient conditions make it cheap and easy for long-term storage. In addition, methanol can be produced from renewable energies and captured carbon dioxide (CO_2), which benefits from the extensive studies of power-to-methanol technology [2–4]. Moreover, lower reforming temperature (473 –573 K) than other carbon-based fuels such as methane (1073 –1273 K) makes it suitable for stack integration with HT-PEM fuel cells and results in a lower CO production [1,5]. Compared to other catalytic reactions for hydrogen production, such as methanol decomposition (MD) and partial oxidation of methanol (POM), the methanol steam reforming (MSR) process provides the highest concentration of hydrogen per mole of methanol [6]. Therefore, the on-board hydrogen generation by MSR becomes an efficient and practical option to fuel PEM fuel cells especially for vehicle propulsion. In the MSR process, the methanol and water (steam) mixture is converted into a hydrogen-rich gas by chemical reactions occurring on the surface of catalysts. The three main reactions for the catalytic MSR process can be written as [7,8]:

Methanol steam reforming (MSR) reaction:

$$CH_3OH + H_2O \leftrightarrow CO_2 + 3H_2 \quad \Delta H = +49.7\left(kJmol^{-1}\right) \tag{1}$$

Water-gas shift (WGS) reaction:

$$CO + H_2O \leftrightarrow CO_2 + H_2 \quad \Delta H = -41.2\left(kJmol^{-1}\right) \tag{2}$$

Methanol decomposition (MD) reaction:

$$CH_3OH \leftrightarrow CO + 2H_2 \quad \Delta H = +90.2\left(kJmol^{-1}\right) \tag{3}$$

The mechanism and kinetics of MSR have been fully investigated both theoretically and experimentally [7–10]. Jiang et al. [11,12] derived an overall power-law and a Langmuir–Hinshelwood-Hougen-Watson rate expressions for the MSR process based on only one type of active site. They neglected the WGS reaction, assuming that the competitive adsorption on the single active site favoured methanol and methyl formate rather than CO. On the contrary, Lee et al. [13] assumed that the MD reaction was negligible and that the CO was produced by the reverse water gas shift (rWGS) reaction. Besides, Peppley et al. [7,8] developed a comprehensive model considering MSR, WGS, and MD reactions over a $CuO/ZnO/Al_2O_3$ catalyst. They proposed two distinct types of active sites: one is for the MD reaction, and another is for the MSR and WGS reactions. More recently, Sá et al. [14] and Herdem et al. [15] compared several kinetic rate expressions for the MSR process over a commercial $CuO/ZnO/Al_2O_3$ catalyst. They found that the kinetic Langmuir-Hinshelwood model based on the work of Peppley et al. [7,8] presented the best agreement with their experimental data.

Due to the fact that the catalyst behaviour is strongly influenced by the reactor geometry and operating conditions, it is critical to develop a numerical model of the chemical reactions and heat and mass transfer phenomena occurring in the packed-bed reactor in order to properly evaluate the reformer performance. Chougule et al. [5] developed a 1D pseudo-homogeneous steady-state model using Engineering Equation Solver (EES) to analyse the MSR process and thermal performance in a tubular packed-bed reactor. However, the wall temperature along the axial direction was assumed to be constant and effectiveness factors were ignorable. These assumptions made it possible to simplify the model. In our early studies [16,17], we developed a 1D pseudo-homogeneous model for the MSR process in a multi-tubular packed-bed reactor without these two simplifying assumptions. This model took into account the effect of interphase and intra-particle transport in the particle scale by introducing effectiveness factors for main reactions. The axial temperature changes on the shell side were also considered, as the burner gas passed through the shell side and provided heat to the tube side in a co-current form. This previously developed 1D model is also used for comparison purposes in the present study.

According to the simulation results of a 1D model, only a few details on actual transport phenomena in reactor tubes were provided, particularly on the radial transport, which may result in a loss of precision when estimating reformer performance [18]. Thus, when significant radial gradients exist in the catalyst bed, it is necessary to develop a 2D model that takes into account both the axial and radial distributions of temperature and

Please cite this article as: Zhu J et al., Comparison between 1D and 2D numerical models of a multi-tubular packed-bed reactor for methanol steam reforming, International Journal of Hydrogen Energy, https://doi.org/10.1016/j.ijhydene.2022.05.109

concentration. Only a few studies, however, have been conducted on the 2D modelling of the MSR process in packed-bed reactors. Ma et al. [19] carried out a 2D pseudo-homogeneous model for the MSR process in a multi-tubular fixed-bed reactor using MATLAB®. They considered the mass and energy balances in both radial and axial directions in the catalyst bed, as well as the axial temperature variation on the shell side. However, even with a $5-6\,mm$ catalyst particle diameter, the effectiveness factors for MSR reactions were ignored. Additionally, the pressure drop along the reactor's length was disregarded. Bayat et al. [20] developed a comprehensive 2D steady-state model for the MSR process over a commercial CuO/ZnO/Al_2O_3 catalyst in a multi-tubular shell-and-tube reactor. A triple-objective optimization of the MSR reformer was performed. However, this model neglected the effectiveness factors for major reactions and the temperature variation on the shell side. Additionally, the effect of the tube size and the formation of hot spots in the catalyst bed were not investigated.

Methods such as computational fluid dynamics (CFD) enable more detailed investigations of the reactor's performance by developing multi-dimensional models [21–24]. However, developing such complicated models is typically computationally expensive and time consuming, with no significant increase in accuracy [9]. Additionally, the benefits of constructing a MATLAB/Simulink-based model may become apparent while carrying out the optimization analysis of a MSR reformer, and further integration with the fuel cell system for the design of control strategy for a reformed methanol fuel cell (RMFC) system.

Most comprehensive models of the MSR process mentioned above neglected the effectiveness factors for key reactions and the temperature variation on the shell side. Besides, the formation of hot spots in catalyst beds, which should be kept within acceptable limits to avoid thermal sintering of catalysts, was not thoroughly investigated. Furthermore, the comparison study between the 1D and 2D models of the MSR process has rarely been conducted, e.g., in the aspects of the effect of radial distributions of temperature and concentration in reactor tubes, and acceptability of the computationally cheaper 1D model under different tube geometry and operating conditions.The present work aims to compare the simulation results of the simplified 1D model and the 2D model in predicting the performance of the reformer. A numerical study of the heat and mass transfer processes coupled with the reaction kinetics in the catalyst bed is conducted using MATLAB®. The thermal behaviour along the axial direction on the shell side is also considered. To validate the proposed kinetic model together with effectiveness factors, the experiment for the MSR process in a small-scale packed-bed reactor is conducted. A 2D steady-state pseudo-homogeneous model is developed considering the temperature and concentration distributions in both axial and radial coordinates. For comparison purposes, a 1D pseudo-homogeneous model of the plug-flow MSR reactor is also developed without taking into account radial gradients. According to the simulation results, the impacts of the geometry and operating conditions on reformer performance in terms of methanol conversion, CO mole fraction, operating temperature, and maximum temperature difference are investigated. Additionally, a parametric study is carried out to obtain the optimal operating conditions for the reformer.

Modelling approach

The packed-bed reactor is designed to be integrated with a 5 kW HT-PEM fuel cell stack. Fig. 1 illustrates the reactor structure, which consists of baffles and tubes inside a cylindrical shell. The reactor shell is usually surrounded by thermal insulation materials to avoid significant heat loss. Reactor tubes, packed with porous cylindrical catalyst pellets, are arranged in an equilateral triangle tube bundle, and installed inside the shell. The gas from the burner passes through the shell side of the reformer, thereby providing an external heat source to drive the reactions in the catalyst bed. Methanol and water mixture are evaporated before entering the reformer. This gas mixture flows through the catalyst bed in the tube side, where the reforming reactions occur on the solid surface of catalyst particles.

The mathematical model was derived by adopting the following assumptions in this study:

- the absence of axial heat and mass dispersion (plug flow);
- the absence of temperature and concentration gradients between the external surface of the particles and the adjacent layer of fluid (pseudo-homogeneous);
- temperature on the shell side is uniformly distributed in the radial direction;
- the absence of temperature and concentration gradients within catalyst particles;
- uniform size, porosity, and activity of catalyst particles;
- constancy of bed void fraction throughout the entire catalyst bed;
- effectiveness factors for main reactions as a function of Thiele modulus;
- no deactivation of catalysts due to the sintering of catalysts and carbon deposition on the catalytic surface.

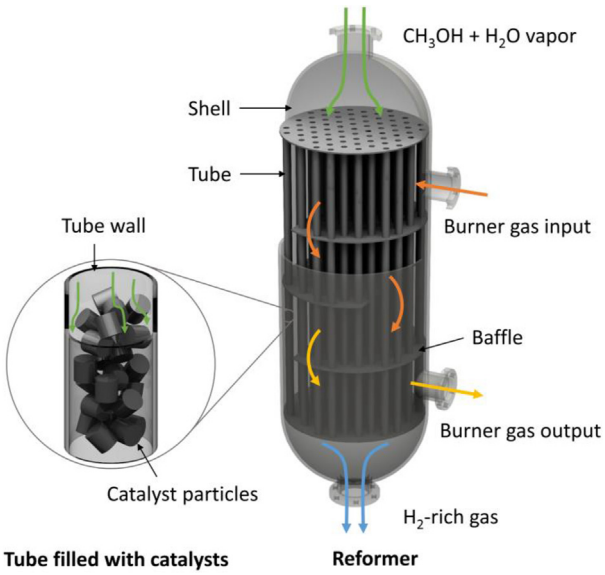

Fig. 1 – Structure of a multi-tubular packed-bed reactor for methanol steam reforming.

Please cite this article as: Zhu J et al., Comparison between 1D and 2D numerical models of a multi-tubular packed-bed reactor for methanol steam reforming, International Journal of Hydrogen Energy, https://doi.org/10.1016/j.ijhydene.2022.05.109

Reaction kinetics

A comprehensive kinetic model developed by Peppley et al. [7,8] was used in this study to describe the MSR process over the $Cu/ZnO/Al_2O_3$ catalyst. The Langmuir-Hinshelwood model is based on assumptions: (a) hydrogen and oxygen-containing species adsorb on different active sites; (b) the active site for the MD reaction is different from that for the MSR and WGS reaction; (c) the rate-determining step (RDS) for both the MSR reaction and the MD reaction is the dehydrogenation of adsorbed methoxy groups; (d) the RDS for the WGS reaction is the formation of an intermediate formate species. The rates r_j (mol $m^{-2}s^{-1}$) for three key reactions (MSR, WGS and MD) involved in the process can be expressed as:

$$r_R = \frac{k_R K^*_{CH_3O^{(1)}} \left(p_{CH_3OH} \Big/ p_{H_2}^{\frac{1}{2}}\right)\left(1 - p_{H_2}^3 p_{CO_2} \Big/ K_R^{eq} p_{CH_3OH} p_{H_2O}\right) C_{S_1}^T C_{S_{1a}}^T}{\left(1 + K^*_{CH_3O^{(1)}}\left(p_{CH_3OH} \Big/ p_{H_2}^{\frac{1}{2}}\right) + K^*_{HCOO^{(1)}} p_{CO_2} p_{H_2}^{\frac{1}{2}} + K^*_{OH^{(1)}}\left(p_{H_2O} \Big/ p_{H_2}^{\frac{1}{2}}\right)\right)\left(1 + K^{\frac{1}{2}}_{H^{(1a)}} p_{H_2}^{\frac{1}{2}}\right)} \tag{4}$$

$$r_W = \frac{k_W K^*_{OH^{(1)}} \left(p_{CO} p_{H_2O} \Big/ p_{H_2}^{\frac{1}{2}}\right)\left(1 - p_{H_2} p_{CO_2} \Big/ K_W^{eq} p_{CO} p_{H_2O}\right) C_{S_1}^{T^2}}{\left(1 + K^*_{CH_3O^{(1)}}\left(p_{CH_3OH} \Big/ p_{H_2}^{\frac{1}{2}}\right) + K^*_{HCOO^{(1)}} p_{CO_2} p_{H_2}^{\frac{1}{2}} + K^*_{OH^{(1)}}\left(p_{H_2O} \Big/ p_{H_2}^{\frac{1}{2}}\right)\right)^2} \tag{5}$$

$$r_D = \frac{k_D K^*_{CH_3O^{(2)}} \left(p_{CH_3OH} \Big/ p_{H_2}^{\frac{1}{2}}\right)\left(1 - p_{H_2}^2 p_{CO} \Big/ K_D^{eq} p_{CH_3OH}\right) C_{S_2}^T C_{S_{2a}}^T}{\left(1 + K^*_{CH_3O^{(2)}}\left(p_{CH_3OH} \Big/ p_{H_2}^{\frac{1}{2}}\right) + K^*_{OH^{(2)}}\left(p_{H_2O} \Big/ p_{H_2}^{\frac{1}{2}}\right)\right)\left(1 + K^{\frac{1}{2}}_{H^{(2a)}} p_{H_2}^{\frac{1}{2}}\right)} \tag{6}$$

where k_j ($m^2 s^{-1} mol^{-1}$) and K_j^{eq} are the rate constant and the equilibrium constant of reaction j, respectively; K^* ($bar^{-0.5}$) is the adsorption coefficient; p_i (bar) is the partial pressure of component i ($i = CO_2, CO, H_2, CH_3OH$ and H_2O); and $C_{S_1}^T$, $C_{S_{1a}}^T$, $C_{S_2}^T$ and $C_{S_{2a}}^T$ (mol m^{-2}) are the total site concentrations of site '1', '1a', '2', and '2a', respectively, where the '1' and '1a' sites are assumed to be active for the MSR and WGS reactions and the '2' and '2a' sites are for the MD reaction. Further details on the calculations of these constants can be found in the Appendix.

The production rate of component i per time per mass of catalyst r_i(mol s^{-1}(kg of catalyst)$^{-1}$) can be calculated considering the rate expression r_j (mol s^{-1} m^{-2}) for individual reaction j and the surface area per unit mass of fresh catalyst S_c(m^2 kg^{-1}) [16]:

$$r_{CO_2} = (r_R + r_W) S_c \tag{7}$$

$$r_{CO} = (r_D - r_W) S_c \tag{8}$$

$$r_{H_2} = (3r_R + 2r_D + r_W) S_c \tag{9}$$

$$-r_{CH_3OH} = (r_R + r_D) S_c \tag{10}$$

$$-r_{H_2O} = (r_R + r_W) S_c \tag{11}$$

Effectiveness factor

The effectiveness factor, η, is estimated as the ratio of the actual reaction rate in the catalyst particle to the calculated rate that exist in the absence of diffusion limitations [25]. In our previous study [17], the Thiele modulus method and the intraparticle distribution methods were applied and compared for predicting the effectiveness factors for main reactions of MSR. The comparison results indicated that both methods could be used when the diameter of cylindrical catalyst particles is set to 1.5 mm. For a first-order reaction in a spherical catalyst pellet, an easier expression for the effectiveness factor η as a function of the Thiele modulus can be derived as [26]:

$$\eta = \frac{3}{\varphi_1^2}(\varphi_1 \coth \varphi_1 - 1) \tag{12}$$

where φ_1 is the Thiel modulus for a first-order reaction, which can be expressed as:

$$\varphi_1^2 = \frac{r_{jp} \rho_c r_p^2 S_c}{D_{i,ep} c_{ip}} \tag{13}$$

where r_{jp} (mol m^{-2} s^{-1}) and c_{ip} (mol m^{-3}) are the rate of reaction j and the concentration of component i, respectively, if the entire interior surface is exposed; r_p (m) is the radius of the catalyst pellet; and ρ_c (kg m^{-3}) is the density of catalyst bed.

Catalysts in the form of porous cylindrical particles with an aspect ratio of 1 are utilized in this study. For a non-spherical particle, the volume-equivalent particle diameter d_p^v (m), defined as the diameter of a single spherical pellet having the same volume as the non-spherical particle, is usually used instead of its actual diameter d_p (m). For a cylinder catalyst with a diameter of d (m) and a height of h (m), the volume-equivalent particle diameter d_p^v can be calculated by:

Please cite this article as: Zhu J et al., Comparison between 1D and 2D numerical models of a multi-tubular packed-bed reactor for methanol steam reforming, International Journal of Hydrogen Energy, https://doi.org/10.1016/j.ijhydene.2022.05.109

$$d_p^v = \left(\frac{6V_{pa}}{\pi}\right)^{\frac{1}{3}} = d\left(\frac{3}{2}\frac{h}{d}\right)^{\frac{1}{3}} \quad (14)$$

where V_{pa} is the volume of a single catalyst particle (m^3).

Steady-state mass and heat balance equations on the tube side

To predict the MSR performance in the plug-flow reactor, two steady-state models (1D and 2D) considering the typical transport and chemical reaction phenomena in the catalyst bed are developed in this study. For the 1D model, it is assumed that no axial mixing occurs in the plug-flow reactor, and the radial gradients are neglected. For the 2D model, the heat and species dispersions in the radial direction are considered. Therefore, uniform temperature and concentration distributions in the cross-section can be estimated.

One-dimensional plug flow

Mass balance

$$u_s\frac{dc_i}{dz} = \eta_i\rho_c r_i \quad (15)$$

where c_i (mol m^{-3}) is the concentration of component i in the fluid, u_s (m s^{-1}) is the superficial velocity of the fluid in axial direction, ρ_c(kg m^{-3}) is the density of catalyst bed, and r_i(mol s^{-1}(kg of catalyst)$^{-1}$) is the rate of consumption or formation of the component i.

Energy balance

$$u_s\rho_f C_{p,f}\frac{dT_t}{dz} = a_s U_t \Delta T + \sum \eta_j\rho_c(-\Delta H_j)r_j S_c \quad (16)$$

where $C_{p,f}$ (J $kg^{-1}K^{-1}$) is the specific heat specific heat of pseudo-fluid, ρ_f (kg m^{-3}) is the pseudo-fluid density, ΔH_j (J mol^{-1}) is the enthalpy change of reaction j, ΔT(K) is the temperature difference between shell side and tube side at length z(m), a_s (m^2 m^{-3}) is the surface-to-volume ratio of a single tube, U_t($Wm^{-2}K^{-1}$ or $Js^{-1}m^{-2}K^{-1}$) is the overall heat transfer coefficient in the tube side.

Two-dimensional plug flow

Fig. 2 displays the schematic diagram of a single reactor tube, which is axisymmetric with the inner radius of tubes R_t and the length L. The 2D steady-state model in the catalyst bed is solved in axi-symmetrical cylindrical coordinates with variations of temperature and concentrations in both the axial (z) and radial (r) directions. The variations in the angular direction around the central axis are assumed to be negligible. In this rectangular region, the lower boundary is the line of symmetry (centreline). At the upper boundary, the heat transfer from the shell side to the tube side is accounted for and modelled by using the film theory. The uniform initial conditions are given at the left boundary. The mass and heat balances in the packed-bed reactor with co-current configuration are expressed by the following equations:

Mass balance

$$u_s\frac{\partial c_i}{\partial z} = D_{er}\left(\frac{\partial^2 c_i}{\partial r^2} + \frac{1}{r}\frac{\partial c_i}{\partial r}\right) + \eta_i\rho_c r_i \quad (17)$$

Energy balance

$$u_s\rho_f C_{p,f}\frac{\partial T_t}{\partial z} = \lambda_{er}\left(\frac{\partial^2 T_t}{\partial r^2} + \frac{1}{r}\frac{\partial T_t}{\partial r}\right) + \sum \eta_j\rho_c(-\Delta H_j)r_j S_c \quad (18)$$

where D_{er} (m^2 s^{-1}) is the effective radial mass diffusion coefficient, λ_{er} (W m^{-1} K^{-1}) is the effective thermal conductivity in the radial direction. Further details on the calculation of D_{er} and λ_{er} can be found in the Appendix.

Initial and boundary conditions

$$c = c_0,\ T = T_0 \quad \text{at } z = 0, 0 \le r \le R_t$$

$$\frac{\partial c}{\partial r} = 0 \quad \text{at } r = 0 \text{ and } r = R_t$$

$$\frac{\partial T}{\partial r} = 0 \quad \text{at } r = 0, \text{ all } z$$

$$\frac{\partial T}{\partial r} = -\frac{U_t}{\lambda_{er}}(T - T_s) \quad \text{at } r = R_t$$

In addition, all the tubes within the tube bundle are subject to the same external conditions at the same cross section of the reformer. It means that the temperature profiles within a single tube can represent the performance of all the tubes in the reformer.

Steady-state heat balance equation on the shell side

The reactor tubes are heated by a co-current stream of burner gas on the shell side. The temperature of the burner gas on the shell side was considered as non-isothermal in the axial direction of the reactor. A simple 1D steady-state model is developed in this study to consider the heat balance for the burner gas:

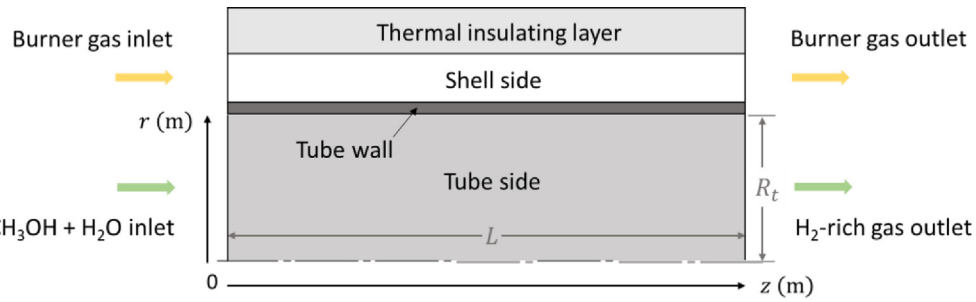

Fig. 2 – Schematic representation of the computational domain in a single packed-bed reactor tube.

Please cite this article as: Zhu J et al., Comparison between 1D and 2D numerical models of a multi-tubular packed-bed reactor for methanol steam reforming, International Journal of Hydrogen Energy, https://doi.org/10.1016/j.ijhydene.2022.05.109

$$u_{s,s}\rho_{f,s}C_{p,s}\frac{dT_s}{dz}=a_sU_s\Delta T \quad (19)$$

where U_s (W $m^{-2}K^{-1}$ or J $s^{-1}m^{-2}K^{-1}$) is the overall heat transfer coefficient in the shell side, $C_{p,s}$ (J $kg^{-1}K^{-1}$) is the specific heat of burner gas, $\rho_{f,s}$ (kg m^{-3}) is the density of burner gas, $u_{s,s}$ (m s^{-1}) is the superficial velocity of the burner gas in the axial direction, D_o(m) is the outer diameter of the tubular reactor, and N_t is the number of tubes in the reformer. The values of parameters in the reformer models can be found in the Table 1. Further details on the model equations can be found in the Appendix.

Simulation method

The model of MSR, in which the concentrations of the major gas species and the temperature in catalyst bed were defined as functions of radial and axial coordinates, was implemented in MATLAB®. For the 2D model, heat and mass transfer phenomena are described by a set of partial differential equations (PDEs). Therefore, the method of lines (MOL) was applied to solve the PDEs in this study [27]. The basic idea of this MOL was to replace the PDE spatial (boundary-value) partial derivatives with algebraic approximations by using finite differences (FDs). In this model, a second-order upwind FD approximation was applied. Thus, with only one remaining independent variable, in this case, a system of ordinary differential equations (ODEs) approximated the original PDE system. Besides, the PDE solver *pdepe* in MATLAB® can also be used for solving the system of PDEs.

Experiments

Experiments for the MSR process were performed at the atmospheric pressure in a small-scale reactor. The reactor was loaded with 3.66 g of the commercial $CuO/ZnO/Al_2O_3$ catalyst in a volume of 3.6 mL. Cylindrical catalyst particles with a diameter of 1.5 mm and an aspect ratio of 1 were used. The feeding rate of the liquid methanol/water mixture from the fuel tank was measured and controlled by a mass flow controller. This mixture was first pumped into an evaporator to be evaporated and preheated. Then the high temperature vapor of fuel passed through the catalyst bed which was supported by a fine mesh grid. The reactor was surrounded by thermal insulation materials and was heated by electric heaters outside the reactor. Therefore, this packed-bed reactor was assumed isothermal. The temperature in the fixed bed was regulated by PID control of the electric heaters to maintain it within a specific range. Two thermocouples were used to measure the inlet and outlet temperatures of the reactor, and the average temperature was regarded as the temperature of the catalyst bed. The main components of the reformate stream from the MSR reactor were analysed by the gas analyser (SIEMENS FIDMAT 6 for CH_3OH, CALOMAT 6 for H_2, and ULTRAMAT 6 for CO and CO_2).

The catalyst bed was firstly flushed with the N_2/H_2 mixture for 1 h, where the volumetric flow rates of H_2 and N_2 were 0.1 cm^3 min^{-1} and 2 cm^3 min^{-1}, respectively. The N_2/H_2 mixture was introduced to the catalyst bed to reduce CuO to Cu (the main active component in the catalyst). The operating temperature for this reduction process was controlled in the range of 433 – 493 K. Therefore, the reduction reaction rate can be kept relatively low so as to avoid any sintering of catalyst. Then, the liquid methanol/water mixture was pumped into the reformer by a dosing pump. The reforming process was carried out with different operating temperatures at 493 K, 513 K and 533 K and the ratio of catalyst weight to the molar flow rate of methanol (W/F_{CH_3OH}) in the range of 44 – 263 kg s mol^{-1}. The variation of W/F_{CH_3OH} was achieved by changing the volumetric flow rate of liquid methanol from 0.051 to 0.308 cm^3 min^{-1} while keeping a fixed loading of catalysts. The S/C was selected to be 1.3 to maximize the methanol conversion without wasting much energy in water evaporation [28].

Table 1 – Properties of catalyst and geometric parameters of the reactor.

Parameter	Value
Density of catalyst bed, ρ_c (kg m^{-3})	1300
BET area, S_c(m^2 kg^{-1})	102000
Average pore diameter Å, (m)	6.4×10^{-9}
Void fraction of catalyst bed, φ	0.37
Diameter of cylindrical catalyst particle, d_p (m)	0.0015
Height of cylindrical catalyst particle, h (m)	0.0015
Site concentrations of site '1', $C^T_{S_1}$ (mol m^{-2})	7.5×10^{-6}
Site concentrations of site '1a', $C^T_{S_{1a}}$ (mol m^{-2})	1.5×10^{-5}
Site concentrations of site '2', $C^T_{S_2}$ (mol m^{-2})	7.5×10^{-6}
Site concentrations of site '2a', $C^T_{S_{2a}}$ (mol m^{-2})	1.5×10^{-5}
Number of reactor tubes, N_t	9
Inner diameter of the tubular reactor, D_i (m)	0.0243
Outer diameter of the tubular reactor, D_o(m)	0.0263
Tube pitch, p_t(m)	0.039
Number of baffle plates, N_b	4
Spacing between baffle plates, p_b (m)	0.12
Length of the reactor, L(m)	0.48
Area fraction of baffle plate that is window, f_b (for 25% baffle plate)	0.1955

Result and discussion

Model validation

Kinetic study for MSR process has been made over a commercial $CuO/ZnO/Al_2O_3$ catalyst. Typically, catalyst kinetic experiments are performed on finely powdered catalysts [5,17]. Hence, obvious diffusion limitations within catalyst particles can be avoided, and the collected reaction rates could be referred to as intrinsic. However, cylindrical catalyst particles with a diameter of 1.5 mm were used in this study. Inside the porous catalyst pellets, chemical reactions and heat and mass transfer take place simultaneously. Effectiveness factors were introduced to qualify the effect of intraparticle diffusion limitations on reaction rates. The effectiveness factor describes the relationship between the diffusive reaction rate and the reaction rate in the bulk stream. In this study, the effectiveness factors for MSR, WGS and MD reactions were calculated as a function of Thiele modulus.

To validate the kinetic model and the effectiveness factors, an experiment was conducted in a small-scale reactor loaded

Please cite this article as: Zhu J et al., Comparison between 1D and 2D numerical models of a multi-tubular packed-bed reactor for methanol steam reforming, International Journal of Hydrogen Energy, https://doi.org/10.1016/j.ijhydene.2022.05.109

with catalyst particles for MSR process. Comparisons between the simulation results and the experimental results on the methanol conversion and the mole fraction of CO were carried out with varying W/F_{CH_3OH} in the range of $0-300$ kg s mol^{-1} and operating temperatures at 493 K, 513 K and 533 K. The operating parameters for simulations and experiments are shown in Table 2.

As shown in Fig. 3 (a), there is a good agreement on methanol conversion between the experimental data and the simulation results of the kinetic model with effectiveness factors. A percentage discrepancy less than 5.4% is observed. The methanol conversion increases with increasing temperature in catalyst bed. In addition, increasing the W/F_{CH_3OH} can also improve the methanol conversion. Fig. 3 (b) shows the experimental and simulated mole fractions of CO in the reformate gas with varying temperature in catalyst bed and W/F_{CH_3OH}. As we can see, the CO production increases with respect to W/F_{CH_3OH} in the reactor. As the operating temperature increases, the mole fraction of CO in the reformate gas also increases. This model can approximately predict the CO concentration under most conditions, except for two data points in the experimental results that lie outside the overall distribution of the dataset. These two unexpected jumps of CO concentration occurred when the W/F_{CH_3OH} was 259 kg s mol^{-1} and the temperature was 493 K and 513 K. It might be caused by the non-uniform distributions of temperature and concentration in the reactor. Therefore, the local reaction rates were affected during the experiment. Another possible explanation is that a very small feeding rate of liquid methanol (0.051 cm^{3}min^{-1}) was introduced to obtain a large value of $W/F_{CH_3OH} = 259$ kg s mol^{-1} in the experiment. This small feeding rate of reactants intensified the effect of non-uniform distributions, which hence led to the oscillations of CO production at the large W/F_{CH_3OH} value. Moreover, the large void fraction near the reactor wall was also a possible reason. However, the radial void fraction profile has not been considered in the model.

Table 2 – Geometric and operating parameters for simulations and experiments.

Parameter	Value
Mass of catalyst (g)	3.66
Volume of catalyst bed (mL)	3.6
Feeding rate of methanol liquid (cm^3 min^{-1})	0.051 – 0.308
Temperature (K)	493 – 533
Pressure (bar)	1
Steam/methanol ratio (mol/mol)	1.3
Catalyst size (mm)	1.5 × 1.5
W/F_{CH_3OH} (kg s mol^{-1})	0 – 300

Temperature and methanol conversion distribution

In the 1D steady-state model, the absence of radial variations in velocity, concentration, temperature, and reactions is assumed in the tubular packed-bed reactor. To better understand the temperature and concentration gradients in both the axial and radial directions in the catalyst bed, the 2D model is developed using the axisymmetric coordinate system. Fig. 4 (a) shows the simulated profile of temperature, while Fig. 4 (b) shows the corresponding profile of methanol conversion in a single reactor tube obtained with the 2D model. In this case, the reformer consists of 9 reactor tubes with the length $L = 0.48$ m, the inner tube diameter $D_t = 32.6$ mm and the thickness of tube wall $x_w = 2$ mm; the catalyst contact time is $W/F_{CH_3OH} = 135$ kg s mol^{-1}; the inlet temperature of the fuel vapor is set as $T_f = 433$ K and the inlet temperature of burner gas is set as $T_b = 673$ K. As shown in Fig. 4 (a), the temperature near the tube wall ($r = R_t$), where the external heat source was applied, shows a sharp increase followed by a gradual drop in the axial direction. The sharp temperature increase is caused by the fact that the inlet temperature of reactants (433 K) is below the inlet temperature of external burner gas (673 K). The substantial temperature difference results to a significant heat transfer from the burner gas. The subsequent temperature drop is due to the strongly endothermic reactions occurring along the catalyst bed. Another reason for this temperature drops along the reactor length is the temperature decrease of the external burner gas. The observed temperature gradients in the radial direction reflect the combined effects of the radial thermal conductivity and the strongly endothermic reactions. A gradual increase of temperature is observed along the central axial line of the tube ($r = 0$ mm). The temperature, then, reaches a relatively stable state, while the radial temperature

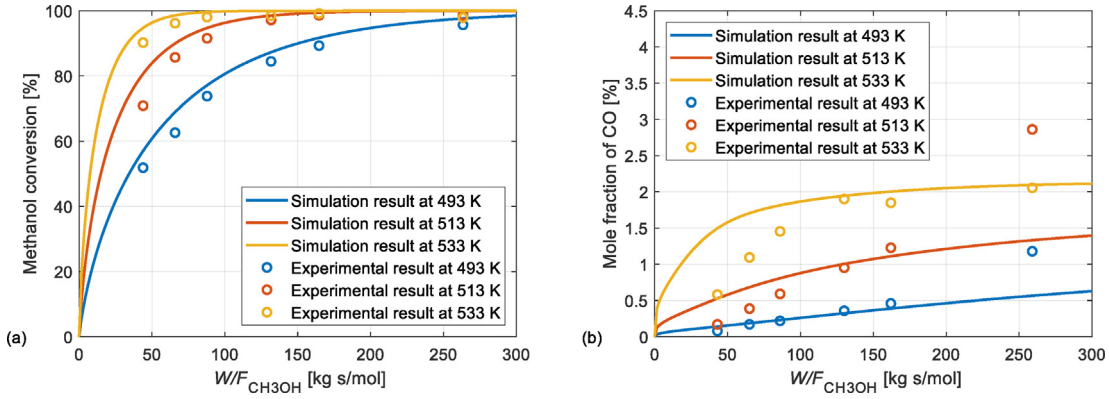

Fig. 3 – Comparison of the (a) methanol conversion and the (b) mole fraction of CO between simulation results and experimental results under different W/F_{CH_3OH} and operating temperatures of catalyst bed.

Please cite this article as: Zhu J et al., Comparison between 1D and 2D numerical models of a multi-tubular packed-bed reactor for methanol steam reforming, International Journal of Hydrogen Energy, https://doi.org/10.1016/j.ijhydene.2022.05.109

distribution becomes nearly uniform. Therefore, a hot spot is most likely to appear near the tube wall and in the early or middle part of the reactor. Under the given conditions, the temperature reaches up to 522.44 K at the hot spot, and the average temperature at the reactor outlet is observed to be 483.00 K. As shown in Fig. 4 (b), the methanol conversion increases along the reactor while the reforming reactions of methanol occur in catalyst bed. The average methanol conversion at the reactor outlet reaches 71.36%.

Fig. 5 shows the comparison of temperature profiles as a function of the radius and length of a single reactor tube predicted by the 1D model and the 2D model. The geometric and operating conditions are the same as in Fig. 4. As shown in Fig. 5 (a), no temperature gradient occurs in the radial direction according to the results of the 1D model. Hence, only a short and rapid temperature increase in the axial direction is observed near the reformer inlet. Afterwards, the temperature increases gradually and eventually reaches a stable state. In comparison, a temperature contour plot obtained by the 2D model is shown in Fig. 5 (b). The radial temperature gradients can be observed, owing to the consideration of effective radial thermal conductivity of catalyst bed. Therefore, the variations of bed temperature can be accurately modelled by the 2D model.

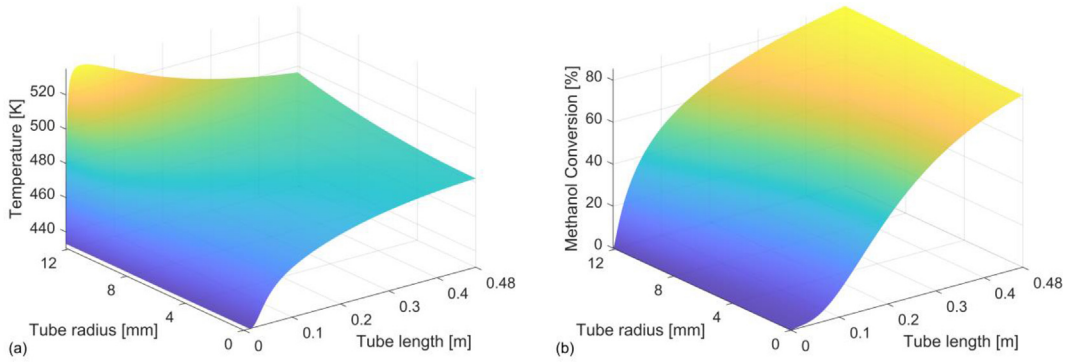

Fig. 4 – Surface plot of (a) temperature and (b) methanol conversion in a single reactor tube by the 2D model: D_t = 24.3 mm, W/F_{CH_3OH} = 135 kg s mol^{-1}, T_b = 673 K.

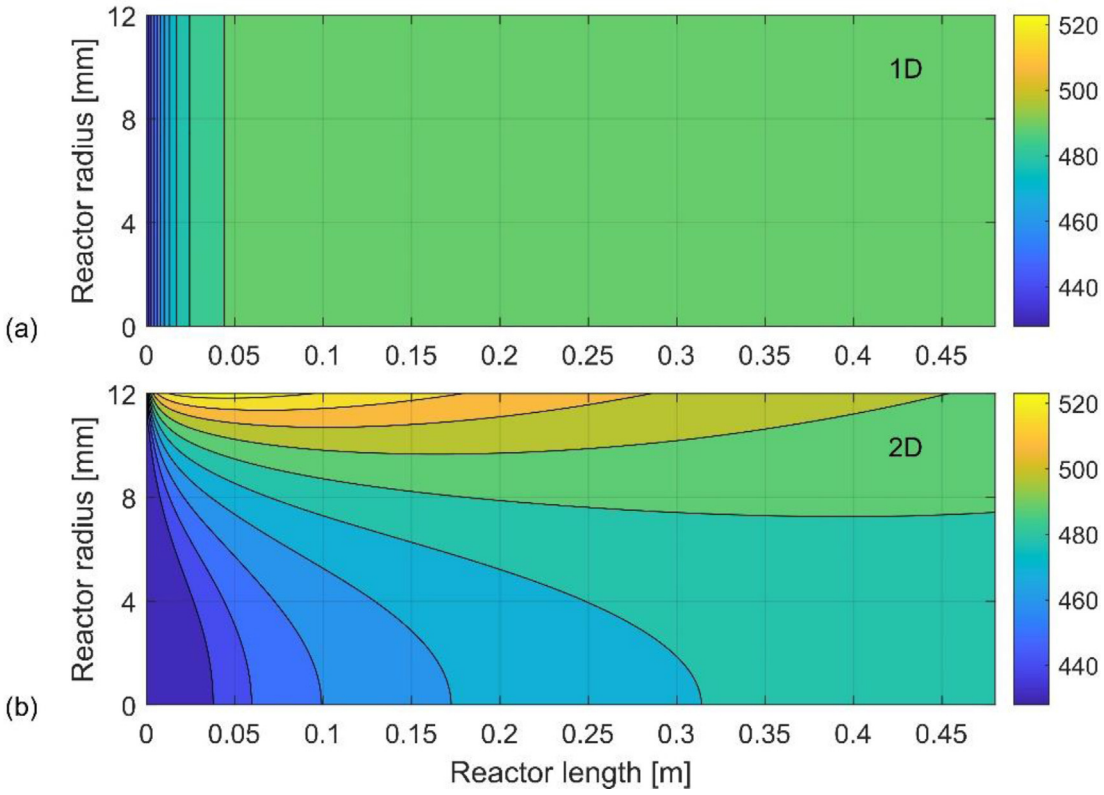

Fig. 5 – Contour plot of temperature in a single reactor tube by the (a) 1D model and the (b) 2D model: D_t = 24.3 mm, W/F_{CH_3OH} = 135 kg s mol^{-1}, T_b = 673 K.

Please cite this article as: Zhu J et al., Comparison between 1D and 2D numerical models of a multi-tubular packed-bed reactor for methanol steam reforming, International Journal of Hydrogen Energy, https://doi.org/10.1016/j.ijhydene.2022.05.109

Effects of geometry and operation conditions

For a 5 kW HT-PEM fuel cell system, the liquid methanol-water mixture with a feeding rate at 4.225 L h^{-1} and a steam-to-carbon ratio (S/C) at 1.3 is provided for hydrogen production. According to the negative effects of impurities on the fuel cells, it is also necessary to limit the mole fraction of CO and methanol to (or less than) 2 – 3% vol and 3% vol in the reformate gas, respectively [29–31]. Therefore, the performance of the reformer should be evaluated to satisfy the requirements of the HT-PEM fuel cell system.

Effect of the inlet temperature of burner gas T_b

The effects of the inlet temperature of burner gas and W/F_{CH_3OH} on axial profiles of methanol conversion and mole fraction of CO are investigated. As shown in Fig. 6, the inlet temperature of burner gas T_b is assigned to be 573 K, 673 K and 773 K, the inner tube diameter D_t is 32.6 mm, the W/F_{CH_3OH} is set as 135 kg s mol^{-1}, while other parameters are kept the same as those of the case in Fig. 4. For the results of 2D model in Fig. 6 (a) and (b), the average methanol conversion at the reactor outlet increases dramatically from 42.0 % to 92.8 %, the average mole fraction of CO produced also increases from 0.35% to 1.20%, while the inlet temperature of burner gas is elevated from 573 K to 773 K. Correspondingly, for the results of 1D model, the methanol conversion at the reactor outlet is improved from 48.6% to 99.3%, and the mole fraction of CO is observed to increase from 0.35% to 1.32%. The distinctions of the methanol conversion and the mole fraction of CO between these two models are owing to the different distributions of temperature calculated in the catalyst bed.

To better understand of the overall temperature activity within the reactor tubes, the axial profiles of the maximum temperature difference of reactor tubes in the radial direction ΔT $(T_{max} - T_{min})$ are illustrated in Fig. 6 (c). In addition, the temperature profiles along the reactor tube at different radial positions are provided in Fig. 7 (a) (b) (c). Due to the radial heat and mass transfer resistances, the thermal behaviour in the catalyst bed evaluated by the 2D model can be different from that which is evaluated by the 1D model. As shown in Fig. 7 (a) (b) (c), the temperature distribution in the catalyst bed is non-uniform and has a sharp rise to the peak near the tube wall in the entrance region. The formation of hot spots could induce the potential risk of local catalyst deactivation due to the thermal sintering. When the inlet temperature of burner gas increases from 573 K to 773 K, the hot-spot temperature

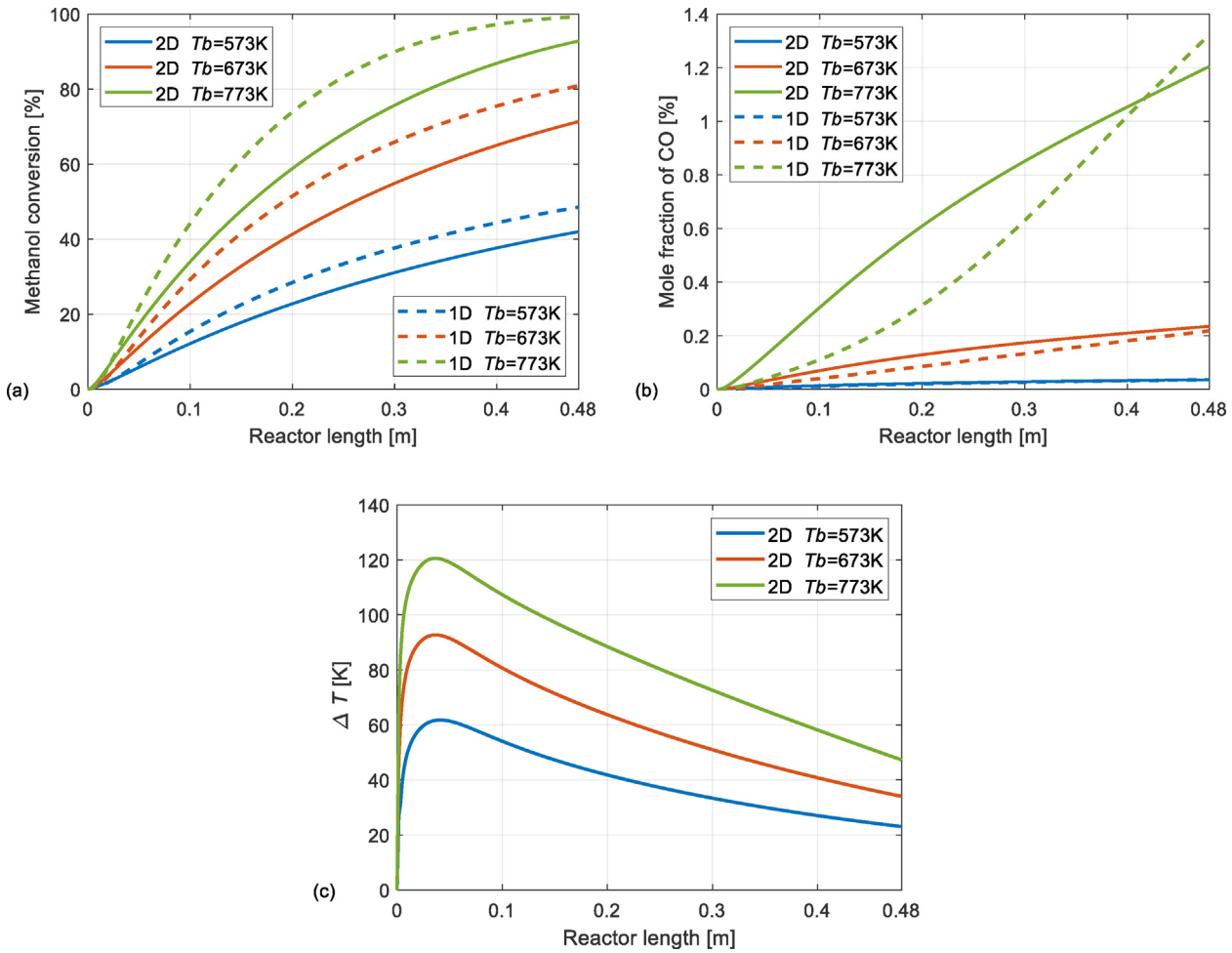

Fig. 6 – Effect of the inlet temperature of burner gas T_b on axial profiles of (a) the methanol conversion, (b) the mole fraction of CO, and (c) the maximum temperature difference in radial direction ΔT $(T_{max} - T_{min})$: D_t = 32.6 mm, W/F_{CH_3OH} = 135 kg s mol^{-1}.

Please cite this article as: Zhu J et al., Comparison between 1D and 2D numerical models of a multi-tubular packed-bed reactor for methanol steam reforming, International Journal of Hydrogen Energy, https://doi.org/10.1016/j.ijhydene.2022.05.109

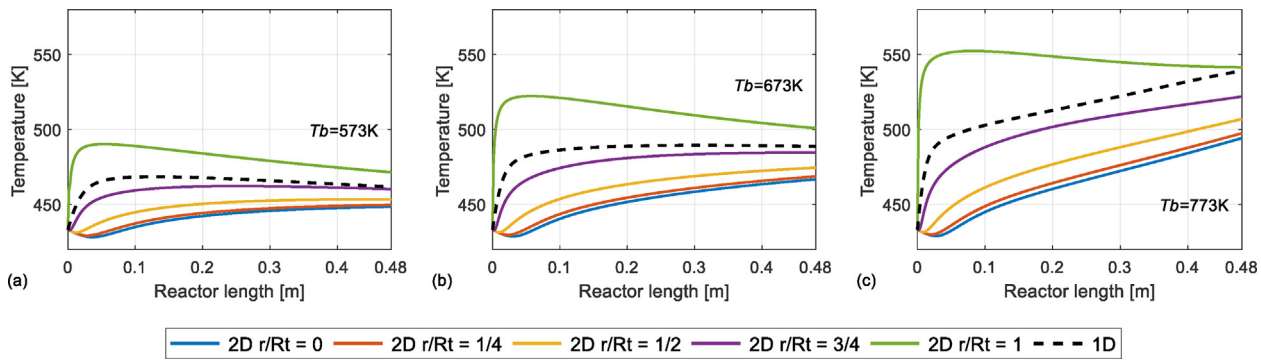

Fig. 7 – Effect of the inlet temperature of burner gas T_b on axial temperature profiles at different radial positions (r/R_t): D_t = 32.6 mm, W/F_{CH_3OH} = 135 kg s mol^{-1}.

observed near the tube wall ($r/R_t = 1$) increases from 490.25 K to 552.40 K. This increase of hot-spot temperature could be caused by the increase of the inlet temperature difference between the shell side and the tube side. It is also observed that the temperature gradient from the tube wall ($r/R_t = 1$) to the tube centre ($r/R_t = 0$) exists in the catalyst bed due to the endothermic reactions and the resistance to heat transfer. As shown in Fig. 6 (c), the elevated inlet temperature of burner gas tends to increase the non-uniformity of the radial temperature distribution in the packed catalyst bed. The reason could be that the higher heat flux amplifies the static temperature gradient along the radial direction.

Effect of the contact time W/F_{CH_3OH}

The increase in W/F_{CH_3OH} means that the surface area of the catalyst in contact with the reactants is increased. Fig. 8 (a) and (b) represent the effects of the W/F_{CH_3OH} on the methanol conversion and the mole fraction of CO along the reactor length, respectively. In this figure, the inlet temperature of burner gas is fixed at 723 K. By varying the tube number in the

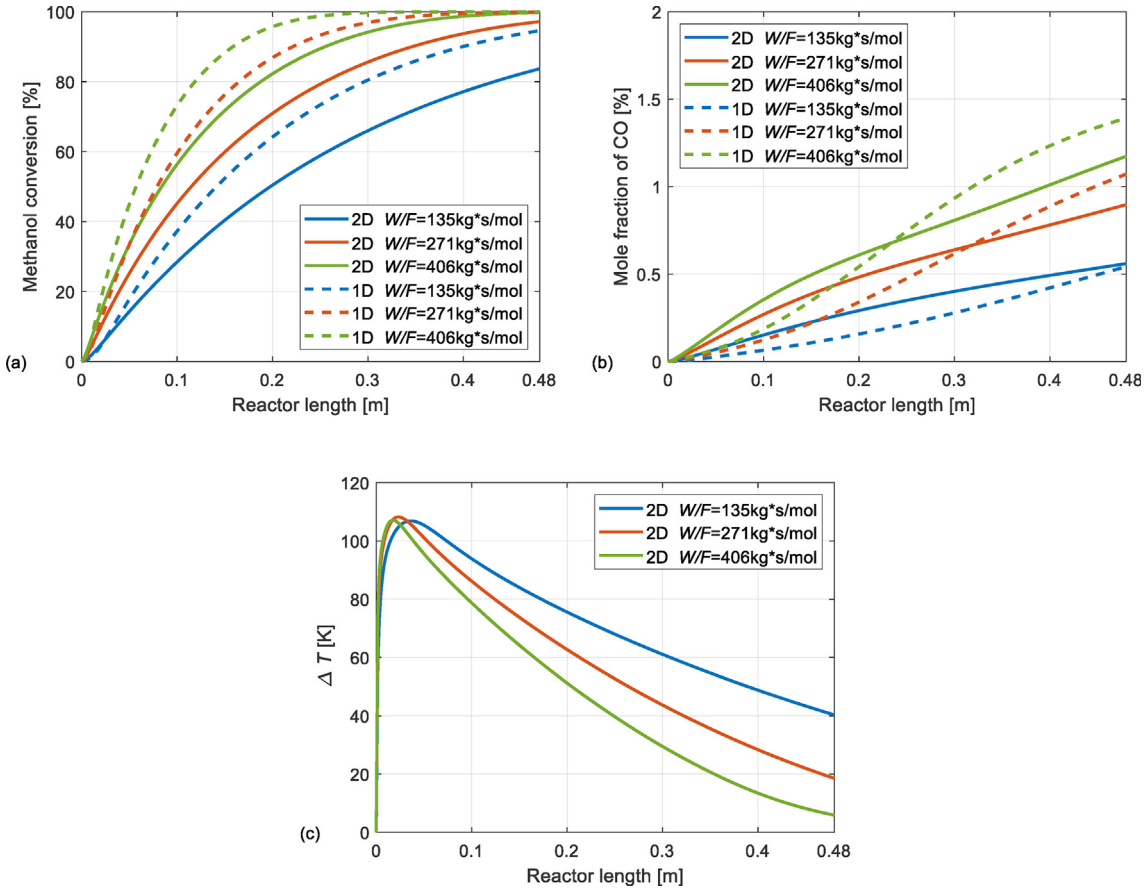

Fig. 8 – Effect of the W/F_{CH_3OH} on axial profiles of (a) the methanol conversion, (b) the mole fraction of CO, and (c) the maximum temperature difference in radial direction ΔT $(T_{max} - T_{min})$: D_t = 32.6 mm, T_b = 723 K.

Please cite this article as: Zhu J et al., Comparison between 1D and 2D numerical models of a multi-tubular packed-bed reactor for methanol steam reforming, International Journal of Hydrogen Energy, https://doi.org/10.1016/j.ijhydene.2022.05.109

reformer while keeping both the tube diameter D_t and tube length L constant, the value of W/F_{CH_3OH} is changed without changing the fuel feeding rate. Based on the results of the 2D model, the average methanol conversion at the reactor outlet is improved from 83.7% to 99.7% as the W/F_{CH_3OH} increases from 135 to 406 kg s mol^{-1}. Correspondingly, the average mole fraction of CO at the reactor outlet increases from 0.56% to 1.17%. For the results of the 1D model, the methanol conversion increases from 93.2% to 100%, and the mole fraction of CO increases from 0.55% to 1.36% while the W/F_{CH_3OH} increases from 135 to 406 kg s mol^{-1}. These results indicate that the rate of the MSR reactions is increased due to the higher values of W/F_{CH_3OH}. It is also shown that, when the methanol conversion is approaching 100%, the differences in methanol conversion and mole fraction of CO between these two models become less significant. Fig. 8 (c) represents the effects of the W/F_{CH_3OH} on axial profiles of the maximum temperature difference in the radial direction ΔT $(T_{max} - T_{min})$ of reactor tubes. The change in W/F_{CH_3OH} is proved to have no significant effect on the highest value of the maximum temperature difference in the radial direction ΔT $(T_{max} - T_{min})$ over the entire reactor.

Fig. 9 demonstrates the comparison of temperature profiles obtained from the 1D model and the 2D model under different W/F_{CH_3OH}. It is shown that the radial temperature gradient at the reactor outlet becomes shallower with the increase of W/F_{CH_3OH}. Fig. 8 (a) indicates that, as the W/F_{CH_3OH} increases to 406 kg s mol^{-1}, the rate of methanol steam reforming reactions becomes greater. The increased reaction rates lead to a higher methanol conversion in the catalyst bed. While the methanol conversion approaches 100%, the speed of the endothermic reactions gradually slows down. Therefore, the temperature in the radial direction can become more uniformly distributed at the reactor outlet, as shown in Fig. 9 (c).

Effect of the tube diameter D_t

The successful design of a polite-scale MSR reformer is to obtain a high methanol conversion and low CO concentration in the hydrogen-rich reformate. In this section, the possibility of adopting fewer reactor tubes with a larger diameter in the multi-tubular packed-bed reformer is investigated in this study. For a reformer with a fixed catalyst inventory, both the number of tubes and the number of welding operations can be inversely proportional to the square of the diameteir. Therefore, the use of large-diameter tubes would reduce the investment cost of the reactor [32]. However, the inner diameter of reactor tubes can profoundly affect the temperature non-uniformity in the catalyst bed. Hence, the 2D model was developed in this study to estimate the effect of tube diameter D_t on the reformer performance.

Fig. 10 (a) and (b) represent the effect of the tube diameter D_t and the inlet temperature of burner gas T_b on the methanol conversion and the mole fraction of CO of the reformer. As the inner tube diameter D_t increases from 13.3 mm to 42.1 mm, the number of tubes should be changed from 60 to 6 to maintain the same overall catalyst load in the reactor. Therefore, the W/F_{CH_3OH} is kept constant at 271 kg s mol^{-1}. Fig. 10 (c) and (d) represent the effect of the tube diameter D_t, and the W/F_{CH_3OH} on the methanol conversion and the mole fraction of CO of the reformer. In Fig. 10 (c) and (d), the inlet temperature of burner gas is kept constant at 673 K, while the W/F_{CH_3OH} is set as 135– 405 kg s mol^{-1}. It is observed that a decrease in diameter leads to an increase in the methanol conversion for this externally heated multi-tubular reactor. The reason could be that, for a small tube diameter, the external heat source can provide sufficient heat throughout the reactor during operation, allowing for relatively ideal diffusion and chemical kinetics to reach a higher methanol conversion. Fig. 10 also indicates that, in these cases, a smaller difference of the methanol conversion (less than 1.74%) between these two models can be observed when the tube diameter decreases to 13.3 mm due to the smaller radial temperature gradients. Therefore, in these cases, it could be concluded that it is sufficient to use a simpler 1D model to estimate the performance of a steam methane reforming reactor when the tube diameter is less than 13.3 mm.

Fig. 10 (e) shows the effect of the tube diameter on axial profiles of the maximum temperature difference in the radial direction ΔT $(T_{max} - T_{min})$ of reactor tubes. In these cases, the W/F_{CH_3OH} is kept constant at 271 kg s mol^{-1}, and the inlet temperature of burner gas is set at 723 K. It is apparent from this figure that the increased tube diameter tends to increase the non-uniformity of the radial temperature distribution in the packed catalyst bed. When the inner diameter is 15.5 mm, the maximum radial temperature difference of 97.5 K is developed in the reactor tube; and when the inner diameter is increased to 42.1 mm, a maximum radial temperature difference of 116.1 K is observed.

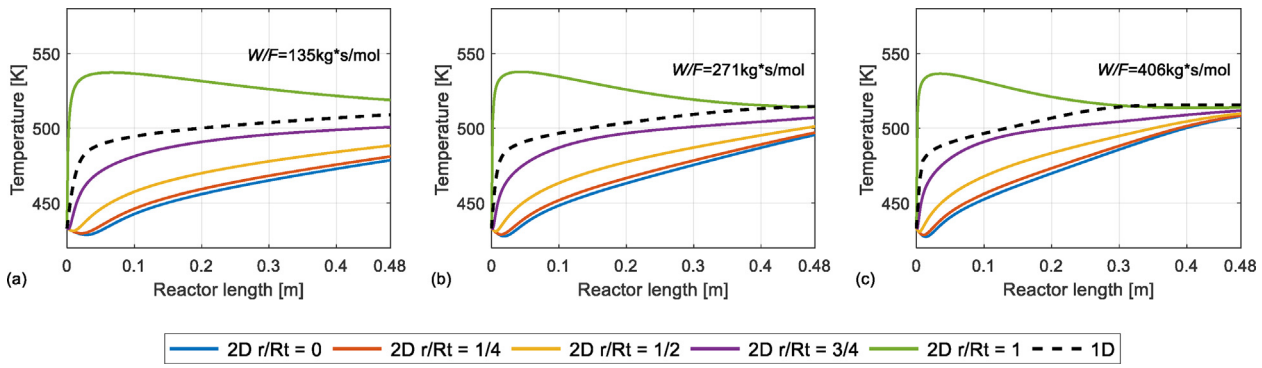

Fig. 9 – Effect of the W/F_{CH_3OH} on axial temperature profiles at different radial positions (r/R_t): $D_t = 32.6$ mm, $T_b = 723$ K.

Please cite this article as: Zhu J et al., Comparison between 1D and 2D numerical models of a multi-tubular packed-bed reactor for methanol steam reforming, International Journal of Hydrogen Energy, https://doi.org/10.1016/j.ijhydene.2022.05.109

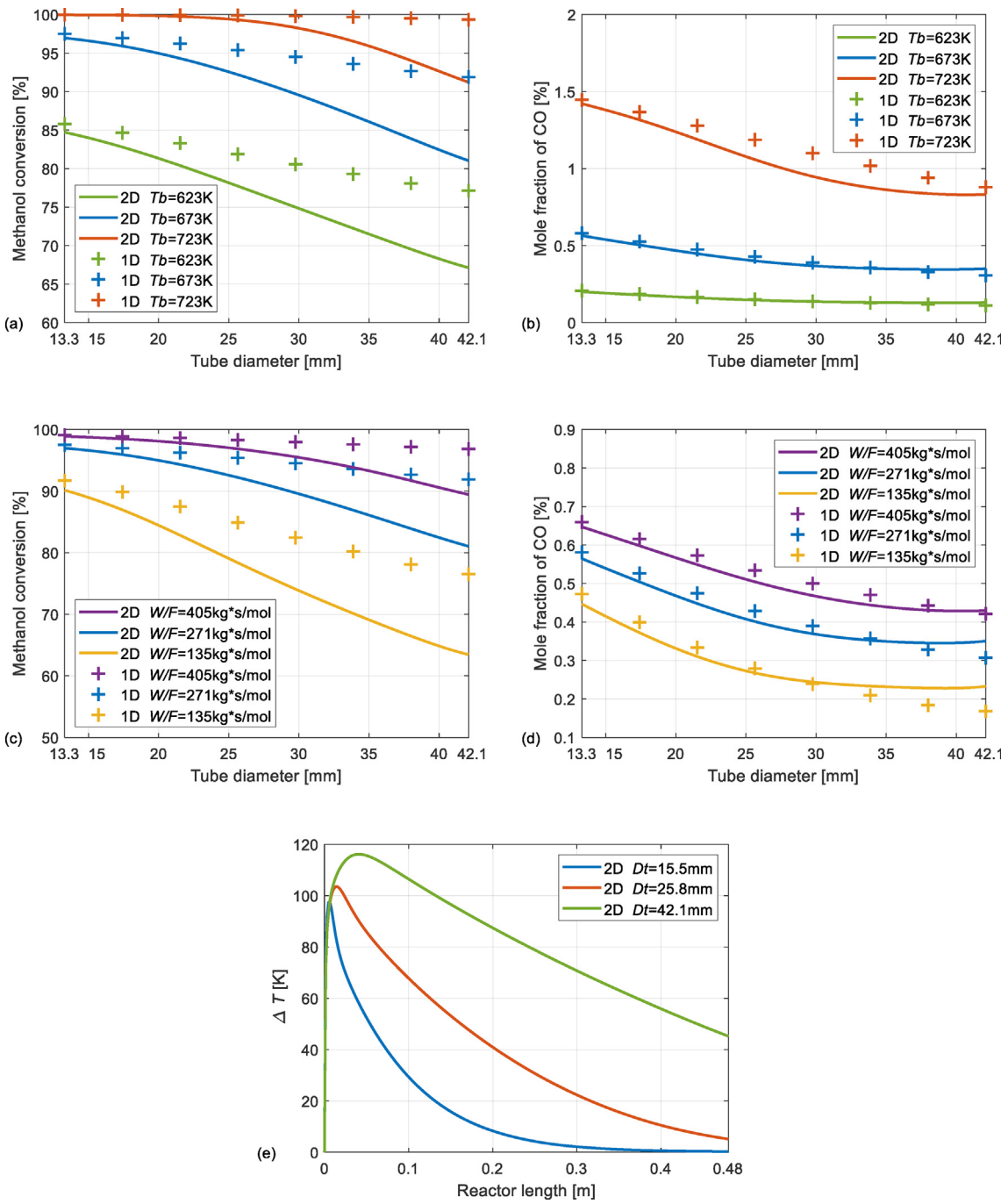

Fig. 10 – Effect of the tube diameter D_t and the inlet temperature of burner gas T_b on axial profiles of (a) the methanol conversion, and (b) the mole fraction of CO: $W/F_{CH_3OH} = 271$ kg s mol^{-1}; effect of the tube diameter D_t and the W/F_{CH_3OH} on axial profiles of (c) the methanol conversion, and (d) the mole fraction of CO: $T_b = 673$ K; and effect of the tube diameter D_t on axial profiles of (e) the maximum temperature difference in radial direction ΔT ($T_{max} - T_{min}$): $T_b = 723$ K, $W/F_{CH_3OH} = 271$ kg s mol^{-1}.

To better understand the overall temperature activity within the reactor tubes, the temperature profiles estimated by the 1D model and the 2D model are provided in Fig. 11. Due to the endothermicity of the MSR process, the lowest temperature appears at the centre of the reactor tube. Besides, the hot spot arises near the tube wall in the entrance region of the reactor due to the peak heat flux. It is also visible in Fig. 11 (a) and (b) and (c) that large tube diameters can enhance the radial temperature gradients when analysing the temperature profiles in the catalyst bed. This phenomenon implies that the heat transfer will be more efficient with the decrease of tube diameter because the surface area per volume is increased. Hence, the temperature is distributed more evenly over the catalyst bed, and the efficiency of the chemical reactions is improved. These results agree with the findings of Davieau et al. [33] that the reactor configurations with a smaller

Please cite this article as: Zhu J et al., Comparison between 1D and 2D numerical models of a multi-tubular packed-bed reactor for methanol steam reforming, International Journal of Hydrogen Energy, https://doi.org/10.1016/j.ijhydene.2022.05.109

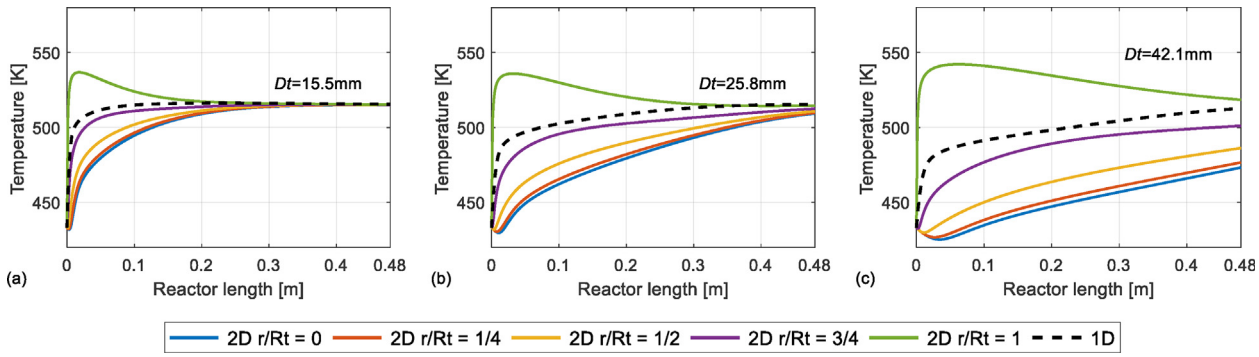

Fig. 11 – Effect of the tube diameter D_t on axial temperature profiles at different radial positions (r/R_t): $T_b = 723$ K, $W/F_{CH_3OH} = 271$ kg s mol^{-1}.

diameter allow a relatively ideal diffusion and nearly complete methanol conversion in catalyst beds.

Optimization of operating parameters

The operating parameters are sensitive parameters for achieving the optimal performance of the reformer. In this study, the effects of the inlet temperature of burner gas and the W/F_{CH_3OH} are evaluated by characterizing the performance of the reformer using the 2D model. In Fig. 12, the tube diameter is set to 18.2 mm. By choosing a smaller tube diameter, a more uniform radial temperature distribution can be obtained in the catalyst bed. The number of tubes changes from 5 to 40. Correspondingly, the W/F_{CH_3OH} varies from

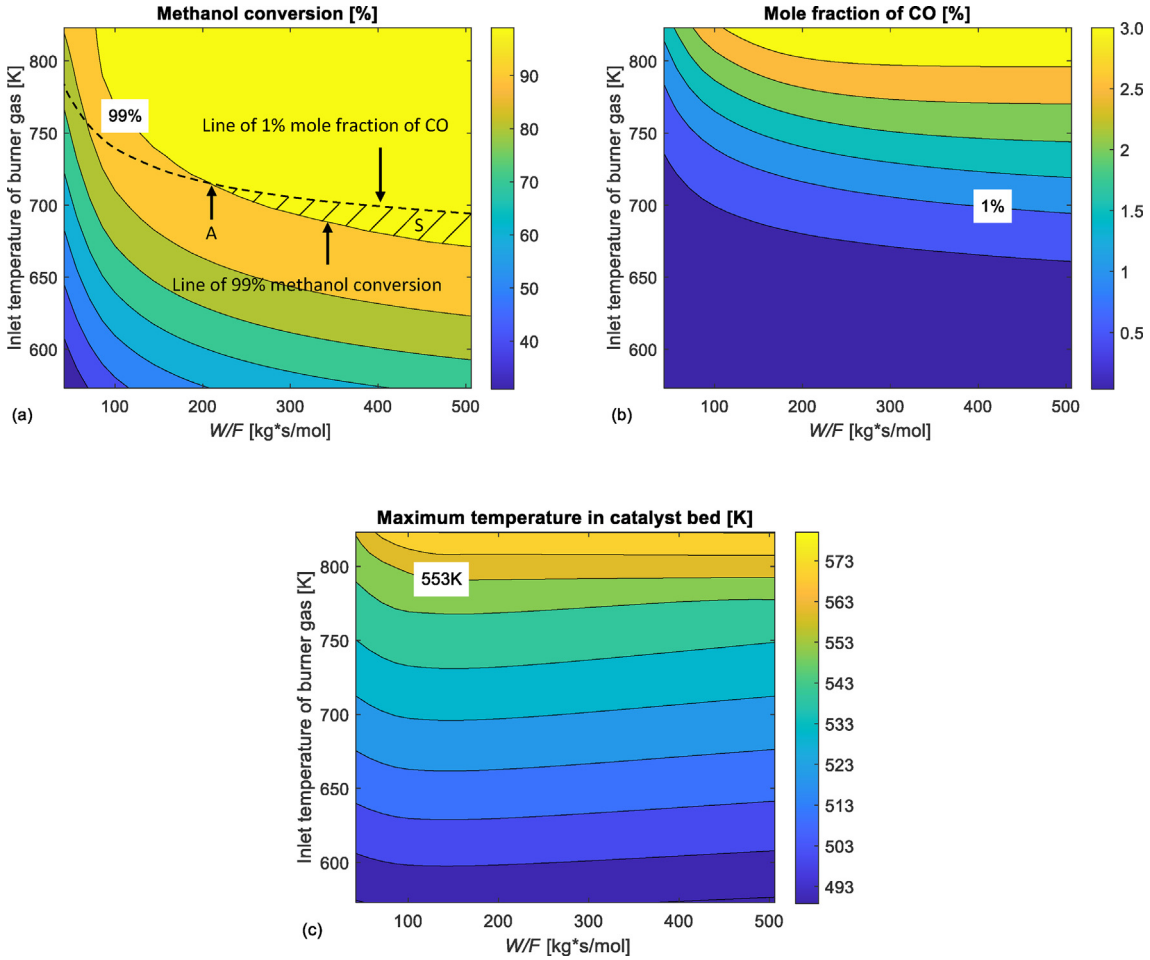

Fig. 12 – Effect of the W/F_{CH_3OH} and the inlet temperature of burner gas on the (a) methanol conversion, (b) mole fraction of CO and (c) maximum hot-spot temperature of the reformer: $D_t = 18.2$ mm.

Please cite this article as: Zhu J et al., Comparison between 1D and 2D numerical models of a multi-tubular packed-bed reactor for methanol steam reforming, International Journal of Hydrogen Energy, https://doi.org/10.1016/j.ijhydene.2022.05.109

42 kg s mol^{-1} to 506 kg s mol^{-1}. As shown in Fig. 12 (a), the methanol conversion can be improved by adopting a higher W/F_{CH_3OH} and a higher inlet temperature of burner gas. The effects of the inlet temperature of burner gas and the W/F_{CH_3OH} on the mole fraction of CO are illustrated in Fig. 12 (b). The results indicate that the increase in the inlet temperature of burner gas and in the W/F_{CH_3OH} will lead to higher CO concentrations in the reformate gas. As shown in Fig. 12 (c), the increase in the inlet temperature of burner gas significantly increases the maximum hot-spot temperature within the catalyst bed.

Based on the demands of an HT-PEM fuel cell system, the reformer should reach a methanol conversion of over 99%. Moreover, the mole fraction of CO in the reformate gas should be limited to a reasonable level (e.g., 1% vol). To prevent the risk of hot-spot formation and subsequent catalyst thermal sintering in certain areas of the reactor, the temperature in catalyst beds should always be kept below the safe limit of 553 K. As shown in Fig. 12 (a), there is a region S that is enclosed by the line of "1% mode fraction of CO" and the line of "99% methanol conversion". Therefore, the operating conditions in the region S can simultaneously bring the methanol conversion to above 99% and the mole fraction of CO to lower than 1% vol in the reformer. Compared with the contour plot in Fig. 12 (c), the operating conditions within the region S also ensure that the maximum hot-spot temperature in the catalyst bed will not exceed the limits of its endurable temperature (553 K). Therefore, it can be concluded that the inlet temperature of burner gas in the range of 671 K to 694 K could be recommended when the W/F_{CH_3OH} is set to 506 kg s mol^{-1}. Additionally, when the W/F_{CH_3OH} is set to 216 kg s mol^{-1}, the inlet temperature of burner gas could be set to 714 K (point A) to minimize the overall catalyst loading in the reformer.

Conclusions

The numerical study comparing a 1D model and a 2D model for the methanol steam reforming process in a multi-tubular packed-bed reformer has been conducted. The steady-state 1D and 2D models have considered the heat and mass transfer processes coupled with the reaction kinetics in the catalyst bed. Besides, the burner gas flowing through the shell side has been modelled as an external heat source using a 1D non-isothermal model. The simulation results of the kinetic model and effectiveness factors have shown good agreement with the experimental data obtained in a small-scale packed-bed reactor for the MSR process. The 1D model has been developed without considering the radial heat and mass transfer. In comparison, the resistances to the radial heat and mass transfer of the reformer tube have been highlighted and introduced in the 2D model.

The simulation results revealed that the overall methanol conversion and the mole fraction of CO in the reformate gas were enhanced by the elevated inlet temperatures of burner gas and W/F_{CH_3OH}. It was also recognized that the overall methanol conversion and the mole fraction of CO in the reformate gas increased as the tube diameter became larger with a fixed catalyst loading in the reformer. Comparisons of the 1D and the 2D models indicated the importance of radial gradients from the centreline to the tube wall in packed-bed reactors. The study showed that the increases in the inlet temperature of burner gas and the tube diameter significantly amplified the maximum radial temperature differences in the catalyst bed. Hot spots were formed near the tube wall in the entrance region. The increase of the inlet temperature of burner gas resulted in a significant increase of the hot-spot temperature inside the catalyst bed. Moreover, with a methanol conversion approaching 100% or a relatively small tube diameter, the simple 1D plug-flow model could be used instead of the 2D model to estimate the performance of the pilot-scale MSR reactor in these cases.

Declaration of competing interest

The authors declare that they have no known competing financial interests or personal relationships that could have appeared to influence the work reported in this paper.

Acknowledgements

The research leading to these results has received funding from the Chinese scholarship council (CSC) and from the Danish Energy Technology Development and Demonstration Program (EUDP) through the Commercial BReakthrough of Advanced fuel cells (COBRA Drive) project, grant number 64018-0118.

Appendix ASupplementary data

Supplementary data to this article can be found online at https://doi.org/10.1016/j.ijhydene.2022.05.109.

Nomenclature

a_s	surface-to-volume ratio, m^2 m^{-3}
C_p	specific heat capacity, J kg^{-1}K^{-1}
$C^T_{S_m}$	total catalyst surface concentration of site m, mol m^{-2}
c_i	concentration of species i, mol m^{-3}
D_{er}	effective radial diffusion coefficient, m^2 s^{-1}
D_i	inner diameter of reactor tube, m
D_o	outer diameter of reactor tube, m
d_p	diameter of catalyst particle, m
d_p^v	volume-equivalent particle diameter, m
E_j	activation energy for rate constant of reaction j, kJ mol^{-1}
f_b	area fraction of baffle plate that is window
h_s	heat transfer coefficient in the shell-side film, W m^{-2} K^{-1}
h_t	heat transfer coefficient in the tube-side film, W m^{-2} K^{-1}
K_i^*	adsorption coefficient of surface species i
K_j^{eq}	reaction equilibrium constant of reaction j
k_j	rate constant for reaction, m^{2}s^{-1}mol^{-1}

M_i	molecular weight of species *i*, kg mol^{-1}
N_b	number of baffle plates
N_t	number of tubes
P	operating pressure, *Pa*
p_b	spacing between baffle plates, m
p_i	partial pressure of species *i*, *Pa*
p_t	tube pitch, m
R	universal gas constant, J $K^{-1}mol^{-1}$
r	radial coordinate, m
r_i	production rate of species *i*, mol $s^{-1}kg^{-1}$
r_j	reaction rate of reaction *j*, mol $m^{-2}s^{-1}$
r_p	radius of the catalyst pellet, m
S_c	surface area per unit mass of fresh catalyst, m^2 kg^{-1}
S/C	steam to carbon molar ratio
T	operating temperature, K
T_b	inlet temperature of burner gas, K
U_t	heat transfer coefficient in the tube side, W $m^{-2}K^{-1}$
U_s	heat transfer coefficient in the shell side, W $m^{-2}K^{-1}$
u_s	superficial velocity, m s^{-1}
W/F_{CH_3OH}	ratio of catalyst weight to the molar flow rate of methanol, kg s mol^{-1}
x_i	mole fraction of species *i*
z	axial position in the tube, m

Greek symbols

μ	viscosity, Pa s
ΔH_j	reaction heat of reaction *j*, J mol^{-1}
ΔT	temperature difference, K
η	effectiveness factor
λ_{er}	effective radial thermal conductivity, W m^{-1} K^{-1}
ρ	density, kg m^{-3}
φ	void fraction of catalyst bed
φ_1	Thiel modulus for a first-order reaction

Superscript and subscript

c	catalyst bed
er	effective radial parameter
i	species including CH_3OH, H_2O, H_2, CO_2 and CO
j	reactions including MSR, WGS and MD
p	catalyst particle
x, y, x	coordinates

REFERENCES

[1] Özcan O, Akın AN. Thermodynamic analysis of methanol steam reforming to produce hydrogen for HT-PEMFC: an optimization study. Int J Hydrogen Energy 2019;44:14117–26. https://doi.org/10.1016/j.ijhydene.2018.12.211.

[2] Léonard G, Giulini D, Villarreal-Singer D. Design and evaluation of a high-density energy storage route with CO2 re-use, water electrolysis and methanol synthesis. In: Comput. Aided chem. Eng, 38. Elsevier; 2016. p. 1797–802.

[3] Cui X, Kær SK, Nielsen MP. Energy analysis and surrogate modeling for the green methanol production under dynamic operating conditions. Fuel 2022;307. https://doi.org/10.1016/j.fuel.2021.121924.

[4] Araya SS, Liso V, Cui X, Li N, Zhu J, Sahlin SL, et al. A review of the methanol economy: the fuel cell route. Energies 2020;13. https://doi.org/10.3390/en13030596.

[5] Chougule A, Sonde RR. Modelling and experimental investigation of compact packed bed design of methanol steam reformer. Int J Hydrogen Energy 2019;44:29937–45. https://doi.org/10.1016/j.ijhydene.2019.09.166.

[6] Chen WH, Su YQ, Lin BJ, Kuo JK, Kuo PC. Hydrogen production from partial oxidation and autothermal reforming of methanol from a cold start in sprays. Fuel 2021;287:1–9. https://doi.org/10.1016/j.fuel.2020.119638.

[7] Peppley BA, Amphlett JC, Kearns LM, Mann RF. Methanol-steam reforming on Cu/Zno/Al2O3. Part 1: the reaction network. Appl Catal A Gen 1999;179:21–9. https://doi.org/10.1016/S0926-860X(98)00298-1.

[8] Peppley BA, Amphlett JC, Kearns LM, Mann RF. Methanol–steam reforming on Cu/ZnO/Al2O3 catalysts. Part 2. A comprehensive kinetic model. Appl Catal A Gen 1999;179:31–49. https://doi.org/10.1016/S0926-860X(98)00299-3.

[9] Pashchenko D. Effect of the geometric dimensionality of computational domain on the results of CFD-modeling of steam methane reforming. Int J Hydrogen Energy 2018;43:8662–73. https://doi.org/10.1016/j.ijhydene.2018.03.183.

[10] Agrell J, Birgersson H, Boutonnet M. Steam reforming of methanol over a Cu/ZnO/Al2O3 catalyst: a kinetic analysis and strategies for suppression of CO formation. J Power Sources 2002;106:249–57.

[11] Jiang CJ, Trimm DL, Wainwright MS, Cant NW. Kinetic mechanism for the reaction between methanol and water over a Cu-ZnO-Al2O3 catalyst. Appl Catal A, Gen 1993;97:145–58. https://doi.org/10.1016/0926-860X(93)80081-Z.

[12] Jiang CJ, Trimm DL, Wainwright MS, Cant NW. Kinetic study of steam reforming of methanol over copper-based catalysts. Appl Catal A, Gen 1993;93:245–55. https://doi.org/10.1016/0926-860X(93)85197-W.

[13] Lee JK, Ko JB, Kim DH. Methanol steam reforming over Cu/ZnO/Al2O3 catalyst: kinetics and effectiveness factor. Appl Catal A Gen 2004;278:25–35. https://doi.org/10.1016/j.apcata.2004.09.022.

[14] Sá S, Sousa JM, Mendes A. Steam reforming of methanol over a CuO/ZnO/Al2O3 catalyst, part I: kinetic modelling. Chem Eng Sci 2011;66:4913–21. https://doi.org/10.1016/j.ces.2011.06.063.

[15] Herdem MS, Mundhwa M, Farhad S, Hamdullahpur F. Multiphysics modeling and heat distribution study in a catalytic microchannel methanol steam reformer. Energy Fuel 2018;32:7220–34. https://doi.org/10.1021/acs.energyfuels.8b01280.

[16] Zhu J, Araya SS, Cui X, Sahlin SL, Kær SK. Modeling and design of a multi-tubular packed-bed reactor for methanol steam reforming over a Cu/ZnO/Al2O3 catalyst. Energies 2020;13:610.

[17] Zhu J, Araya SS, Cui X, Kær SK. The role of effectiveness factor on the modeling of methanol steam reforming over CuO/ZnO/Al2O3 catalyst in a multi-tubular reactor. Int J Hydrogen Energy 2022. https://doi.org/https://doi.org/10.1016/j.ijhydene.2021.12.223.

[18] Rase HF. Fixed-bed reactor design and diagnostics: gas-phase reactions. Butterworth-Heinemann; 2013.

[19] Ma H, Zhou M, Ying W, Fang D. Two-dimensional modeling of a plant-scale fixed-bed reactor for hydrogen production from methanol steam reforming. Int J Hydrogen Energy 2016;41:16932–43. https://doi.org/10.1016/j.ijhydene.2016.07.117.

[20] Bayat M, Garmroodi Asil A. Robust multi-objective optimization of methanol steam reforming for boosting hydrogen production. Int J Hydrogen Energy 2021;46:29795–811. https://doi.org/10.1016/j.ijhydene.2021.06.164.

[21] Wang F, Li L, Liu Y. Effects of flow and operation parameters on methanol steam reforming in tube reactor heated by

Please cite this article as: Zhu J et al., Comparison between 1D and 2D numerical models of a multi-tubular packed-bed reactor for methanol steam reforming, International Journal of Hydrogen Energy, https://doi.org/10.1016/j.ijhydene.2022.05.109

simulated waste heat. Int J Hydrogen Energy 2017;42:26270–6. https://doi.org/10.1016/j.ijhydene.2017.09.002.
[22] Zhuang X, Xu X, Li L, Deng D. Numerical investigation of a multichannel reactor for syngas production by methanol steam reforming at various operating conditions. Int J Hydrogen Energy 2020;45:14790–805. https://doi.org/10.1016/j.ijhydene.2020.03.207.
[23] Wan Z, Yang S, Bao G, Hu J, Wang H. Multiphase particle-in-cell simulation study of sorption enhanced steam methane reforming process in a bubbling fluidized bed reactor. Chem Eng J 2022;429:132461.
[24] Wan Z, Yang S, Hu J, Bao G, Wang H. CFD study of the reactive gas-solid hydrodynamics in a large-scale catalytic methanol-to-olefin fluidized bed reactor. Energy 2022;243:122974.
[25] Cruz BM, da Silva JD. A two-dimensional mathematical model for the catalytic steam reforming of methane in both conventional fixed-bed and fixed-bed membrane reactors for the Production of hydrogen. Int J Hydrogen Energy 2017;42:23670–90. https://doi.org/10.1016/j.ijhydene.2017.03.019.
[26] Fogler HS. Essentials of chemical reaction engineering: Essenti Chemica Reactio Engi. Pearson Education; 2010.
[27] Schiesser WE, Griffiths GW. A compendium of partial differential equation models: method of lines analysis with Matlab. Cambridge University Press; 2009.
[28] Zhuang X, Xia X, Xu X, Li L. Experimental investigation on hydrogen production by methanol steam reforming in a novel multichannel micro packed bed reformer. Int J Hydrogen Energy 2020;45:11024–34. https://doi.org/10.1016/j.ijhydene.2020.02.034.
[29] Zhou F, Andreasen SJ, Kær SK, Park JO. Experimental investigation of carbon monoxide poisoning effect on a PBI/H3PO4 high temperature polymer electrolyte membrane fuel cell: influence of anode humidification and carbon dioxide. Int J Hydrogen Energy 2015;40:14932–41. https://doi.org/10.1016/j.ijhydene.2015.09.056.
[30] Araya SS, Andreasen SJ, Kær SK. Experimental characterization of the poisoning effects of methanol-based reformate impurities on a PBI-based high temperature PEM fuel cell. Energies 2012;5:4251–67. https://doi.org/10.3390/en5114251.
[31] Araya SS, Grigoras IF, Zhou F, Andreasen SJ, Kær SK. Performance and endurance of a high temperature PEM fuel cell operated on methanol reformate. Int J Hydrogen Energy 2014;39:18343–50. https://doi.org/10.1016/j.ijhydene.2014.09.007.
[32] Montebelli A, Visconti CG, Groppi G, Tronconi E, Kohler S. Optimization of compact multitubular fixed-bed reactors for the methanol synthesis loaded with highly conductive structured catalysts. Chem Eng J 2014;255:257–65. https://doi.org/10.1016/j.cej.2014.06.050.
[33] Davieau DD, Erickson PA. The effect of geometry on reactor performance in the steam-reformation process. Int J Hydrogen Energy 2007;32:1192–200. https://doi.org/10.1016/j.ijhydene.2006.11.029.

Please cite this article as: Zhu J et al., Comparison between 1D and 2D numerical models of a multi-tubular packed-bed reactor for methanol steam reforming, International Journal of Hydrogen Energy, https://doi.org/10.1016/j.ijhydene.2022.05.109